Electronic Supplementary Material (ESI) for Nanoscale.
This journal is © The Royal Society of Chemistry 2023

**Supplementary information**

# Galvanic-Replacement-Induced Introduction of an Hetero-ligand into Bimetallic and Trimetallic Nanoclusters

*Jian-Hong Liao,*[a] *Tzu-Hao Chiu,*[a] *Hao Liang,*[b] *Samia Kahlal,*[b] *Jean-Yves Saillard,*[b,*] *and C. W. Liu* [a,*]

[a] Department of Chemistry, National Dong Hwa University, Hualien 974301, Taiwan (Republic of China). E-mail: chenwei@gms.ndhu.edu.tw

[b] Univ Rennes, CNRS, ISCR-UMR 6226, F-35000 Rennes, France. E-mail: jean-yves.saillard@univ-rennes1.fr

## Experimental section

All chemicals used as received were purchased from commercial sources. Solvents were purified following standard protocols.[S1] All reactions were performed in oven-dried Schlenk glassware using standard inert atmosphere techniques. $[AuAg_{20}\{S_2P(O^nPr)_2\}_{12}]PF_6$,[S2] $[PtAg_{20}\{S_2P(O^nPr)_2\}_{12}]$,[S3] and $Au(PPh_3)Cl$[S4] were prepared by procedures reported earlier in literature. The $^1H$ and $^{31}P\{^1H\}$ NMR spectra were recorded on a Bruker Avance II 400 MHz NMR spectrometer, operating at 400.13 MHz for $^1H$, and 161.98 MHz for $^{31}P$. The chemical shifts (δ) and coupling constants (J) are reported in ppm and Hz, respectively. X-ray diffraction data were collected on a Bruker APEX II CCD diffractometer. UV-visible absorption spectra were measured on a Perkin Elmer Lambda 750 spectrophotometer using quartz cells with path length of 1 cm. The emission, lifetime, and quantum yield spectra were recorded on an Edinburgh FLS920 fluorescence spectrometer.

**Synthesis of $[Au@Au_4Ag_{12}\{S_2P(O^nPr)_2\}_7(PPh_3)_4](PF_6)_2$ (1)**

$[AuAg_{20}\{S_2P(O^nPr)_2\}_{12}]PF_6$ (0.1012 g, 0.02 mmol) was dissolved in THF (30 mL), and cooled at -20°C for 10 minutes. $Au(PPh_3)Cl$ (0.04 g, 0.08 mmol) was added and the reaction mixture was kept stirring at the same temperature. After 2h, the solution was dried under a reduced pressure (note that significantly shorter reaction times also yield the product, but with slightly lower yields). The residue was dissolved in $CH_2Cl_2$ (30 mL) and washed with DI-$H_2O$ (3×15 mL). The organic layer was filtered and dried under vacuum to obtain dark red powder. It was further purified by thin-layer chromatography (TLC) plate using a solvent mixture of $Et_2O$ and *n*-hexane (v/v = 1:9). The middle dark orange product was collected to yield $[Au@Au_4Ag_{12}\{S_2P(O^nPr)_2\}_7(PPh_3)_4](PF_6)_2$. Yield: 0.0179 g (17.5%, based on Au). $^{31}P\{^1H\}$ NMR (161.98 MHz, $CDCl_3$, δ, ppm): 102.45 ($S_2P$), 37.2 ($PPh_3$) -143.0 (sept, $^1J_{PF}$ = 709 Hz, $PF_6$). $^1H$ NMR (400.13 MHz, $CDCl_3$, δ, ppm): 0.93 (t, $^3J_{HH}$ = 7.4 Hz, 42H, $CH_3$), 1.71 (m, 28H, $CH_2$), 4.11 (m, 28H, $OCH_2$), 7.49 (m, 80H, $PPh_3$). UV-vis [$\lambda_{max}$ in nm, (ε in $M^{-1}cm^{-1}$)]: 263 (79600), 421 (9700).

**Synthesis of $[Pt@Au_4Ag_{12}\{S_2P(O^nPr)_2\}_7(PPh_3)_4]$ (2)**

$[PtAg_{20}\{S_2P(O^nPr)_2\}_{12}]$ (0.098 g, 0.02 mmol) and $Au(PPh_3)Cl$ (0.04 g, 0.08 mmol) were dissolved in THF (30 mL). The reaction was kept stirring for 5 min and then dried under vacuum. The residue was dissolved in *n*-hexane and filtered. The filtration was evaporated to yield dark red powder as $[Pt@Au_4Ag_{12}\{S_2P(O^nPr)_2\}_7(PPh_3)_4]$. Yield: 0.011 g (10%, based on Au). $^{31}P\{^1H\}$ NMR (161.98 MHz, $d_6$-acetone, δ, ppm): 101.7, 102.5, 104.2 ($S_2P$), 29.8 ($PPh_3$). $^1H$ NMR (400.13 MHz, $d_6$-acetone, δ, ppm): 0.89-1.1 (m, 42H, $CH_3$), 1.72-1.79 (m, 28H, $CH_2$), 3.88-4.21 (m, 28H, $OCH_2$), 7.33-7.73 (m,

60H, $PPh_3$). UV-vis [$\lambda_{max}$ in nm, ($\varepsilon$ in $M^{-1}cm^{-1}$)]: 398 (9700), 425 (8600), 455 (6300), 493 (4500), 540 (2000).

**X-ray crystallography.** Single crystals suitable for X-ray diffraction analysis of **1** were obtained by slow diffusion of *n*-hexane into dichloromethane solution of the compound at 4°C within a week. The single crystals of **2** were obtained by slow diffusion of *n*-hexane into acetone solution at room temperature within two weeks. Single crystals were mounted on the tip of a glass fiber with epoxy resin. Data were collected on a Bruker APEX II CCD diffractometer using graphite monochromated Mo K$\alpha$ radiation ($\lambda$ = 0.71073 Å) at 100K. Absorption corrections for area detector were performed with SADABS[S5] and the integration of raw data frame was performed with SAINT.[S6] The structures were solved by direct methods and refined by least-squares against $F^2$ using the SHELXL-2018/3 package,[S7] incorporated in SHELXTL/PC V6.14.[S8] All non-hydrogen atoms were refined anisotropically. Structure refinements of **2** have been tested by replacing the central Pt with Au. The latter shows slightly higher values in its thermal parameter (from 0.00881 to 0.00923) and wR2 (from 0.0929 to 0.0932), and two refinements were compared based on the same GOF value of 1.024). The test results indicate that placing Au at the center results in a slightly higher electron density than the observed one. Placing Pt at the center matches better with the observed electron density. CCDC no. 2237651 (**1**) and 2237652 (**2**) contain the supplementary crystallographic data for compounds **1** and **2** in this article. These data can be obtained free of charge from The Cambridge Crystallographic Data Centre via www. ccdc.cam.ac.uk/data_request/cif.

**Computational details.** Density Functional Theory (DFT) calculations were carried out using the Gaussian (R) 16 program.[S9] The split valence polarization (def2-SVP) basis set[S10] was used, together with the BP86[S11,S12] exchange-correlation functional, which we kwown it provides reliable ground-state results for metal NCs at a reasonable computational cost. All the optimized structures were confirmed as true minima on their potential energy surface by analytical vibration frequency calculations. Natural atomic orbital (NAO) populations and Wiberg bond indices were computed with the natural bond orbital NBO 6.0 program[S13-S15] implemented in the Gaussian (R) 16 package. The UV-visible transitions were calculated by means of TD-DFT calculations with the same basis set, but with the hybrid B3LYP functional,[S16,S17] which provides more reliable results, although at a higher computational cost, than the BP86 functional. The simulated UV-visible spectra were simulated from the computed TD-DFT transitions and their oscillator strengths by using the SWizard program,[S18] each transition being associated with a Gaussian function of half-height width equal to 3000 $cm^{-1}$.

## References


S1. D. D. Perrin and W. L. F. Armarego, In *Purification of laboratory chemicals*, 3rd Edition, Pergamon Press, Oxford, 1988.

S2. Y.-R. Lin, P. V. V. N. Kishore, J.-H. Liao, S. Kahlal, Y.-C. Liu, M.-H. Chiang, J.-Y. Saillard and C. W. Liu *Nanoscale*, 2018, **10**, 6855.

S3. T.-H. Chiu, J.-H. Liao, F. Gam, I. Chantrenne, S. Kahlal, J.-Y. Saillard and C. W. Liu *J. Am. Chem. Soc.*, 2019, **141**, 12957.

S4. S. S. Zalesskiy, A. E. Sedykh, A. S. Kashin and V. P. Ananikov *J. Am. Chem. Soc.*, 2013, **135**, 3550.

S5. SADABS, version 2014-11.0, Bruker Area Detector Absorption Corrections, Bruker AXS, Inc., Madison, WI, 2014.

S6. SAINT, V8.30A, Software for the CCD Detector System, Bruker Analytical, Madison, WI, 2012.

S7. G. M. Sheldrick *Acta Cryst. A*, 2008, **64**, 112.

S8. SHELXTL, Version 6.14, Bruker AXS, Inc., Madison, Wisconsin, 2003.

S9. M. J. Frisch, G. W. Trucks, H. B. Schlegel, G. E. Scuseria, M. A. Robb, J. R. Cheeseman, G. Scalmani, V. Barone, G. A. Petersson, H. Nakatsuji, X. Li, M. Caricato, A. V. Marenich, J. Bloino, B. G. Janesko, R. Gomperts, B. Mennucci, H. P. Hratchian, J. V. Ortiz, A. F. Izmaylov, J. L. Sonnenberg, D. Williams-Young, F. Ding, F. Lipparini, F. Egidi, J. Goings, B. Peng, A. Petrone; T. Henderson, D. Ranasinghe, V. G. Zakrzewski, J. Gao, N. Rega, G. Zheng, W. Liang, M. Hada, M. Ehara, K. Toyota, R. Fukuda, J. Hasegawa, M. Ishida, T. Nakajima, Y. Honda, O. Kitao, H. Nakai, T. Vreven, K. Throssell, Jr. J. A. Montgomery, J. E. Peralta, F. Ogliaro, M. J. Bearpark, J. J. Heyd, E. N. Brothers, V. N. Kudin, V. N. Staroverov, T. A. Keith, R. Kobayashi, J. K. Normand Raghavachari, A. P. Rendell, J. C. Burant, S. S. Iyengar, J. Tomasi, M. Cossi, J. M. Millam, M. Klene, C. Adamo, R. Cammi, J. W. Ochterski, R. L. Martin, K. Morokuma, O. Farkas, J. B. Foresman and Fox, D. J. *Gaussian, Inc.*, Wallingford CT, 2016; Gaussian 16, Revision A.03.

S10. F. Weigend and R. Ahlrichs. Balanced Basis Sets of Split Valence, Triple Zeta Valence and Quadruple Zeta Valence Quality for H to Rn: Design and Assessment of Accuracy. *Phys. Chem. Chem. Phys*., 2005, **7**, 3297-3305.

S11. A. D. Becke. Density-Functional Exchange-Energy Approximation with Correct Asymptotic Behavior. *Phys. Rev. A.*, 1988, **38**, 3098-3100.

S12. J. P. Perdew. Density-Functional Approximation for the Correlation Energy of the Inhomogeneous Electron Gas. *Phys. Rev. B.*, 1986, **33**, 8822-8824.

S13. A. E. Reed and F. Weinhold. Natural Bond Orbital Analysis of near-Hartree-Fock Water Dimer. *J. Chem. Phys*., 1983, **78**, 4066-4073.

S14. J. E. Carpenter and F. Weinhold. Analysis of the Geometry of the Hydroxymethyl Radical by the Different Hybrids for Different Spins Natural Bond Orbital Procedure. *J. Mol. Struct. (Theochem).,* 1988, **169**, 41-62.

S15. A. E. Reed, L. A. Curtiss and F. Weinhold. Intermolecular Interactions From a Natural Bond Orbital, Donor-Acceptor Viewpoint. *Chem. Rev*., 1988, **88**, 899-926.

S16. A. D. Becke. Density-functional thermochemistry. III. The Role of Exact Exchange. *J. Chem. Phys.*, 1998, **98**, 5648-5652.

S17. P. J. Stephens, F. J. Devlin, C. F. Chabalowski and M. J. Frisch. Ab Initio Calculation of Vibrational Absorption and Circular Dichroism Spectra Using Density Functional Force Fields. *J. Phys. Chem.*, 1994, **98**, 11623-11627.

S18. S. I. Gorelsky. SWizard program, revision 4.5, http://www.sg-chem.net.

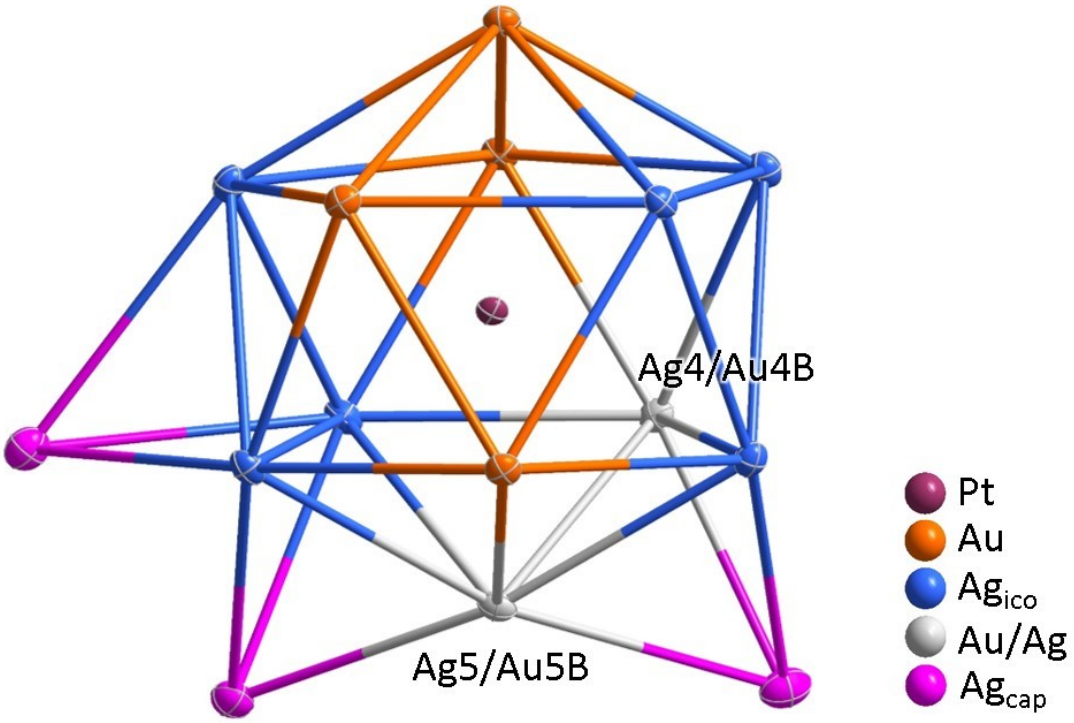


| Occupancy | Ag4/Au4B | Ag5/Au5B |
|---|---|---|
| Ag | 0.85 | 0.90 |
| Au | 0.15 | 0.10 |

**Figure S1.** The detailed refinement of the occupancy factor of the fifth Au atom disordered at two positions in structure **2b**.

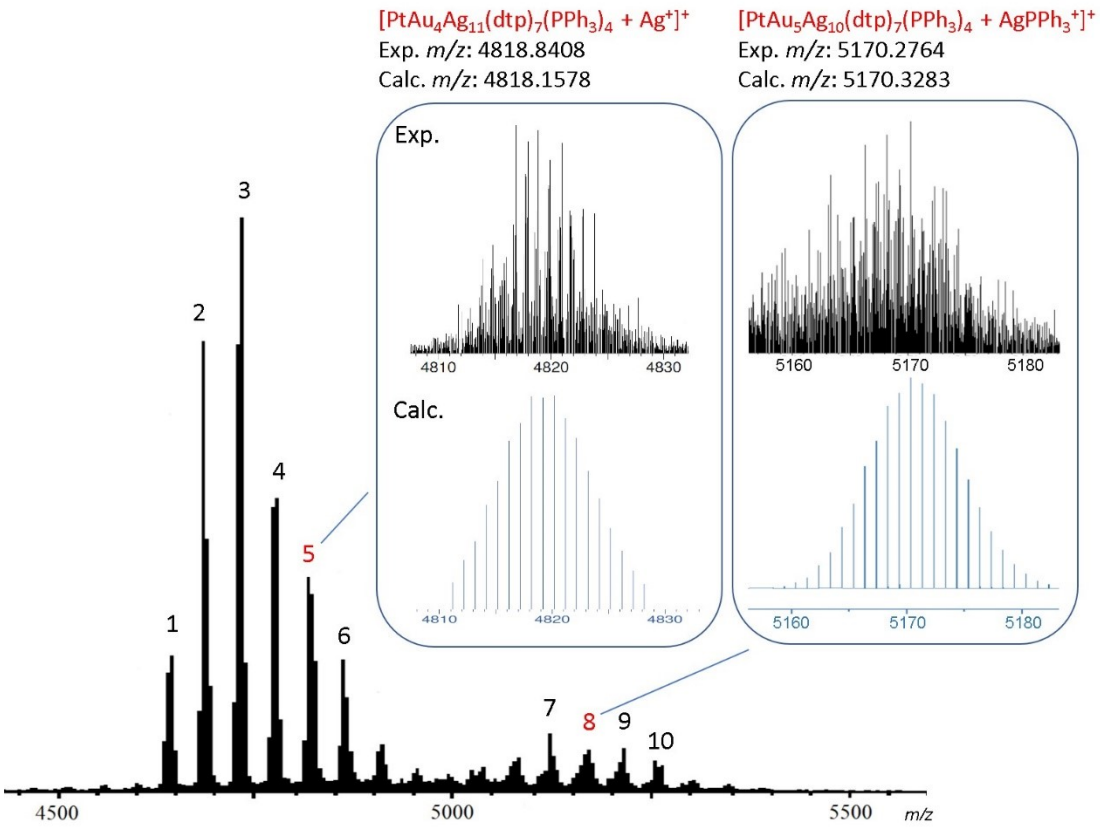


| | Molecular ion | Exp. (*m/z*) | Calc. (*m/z*) |
|---|---|---|---|
| 1 | $[PtAg_7(dtp)_7(PPh_3)_8 + Ag^+]^+$ | 4642.9092 | 4648.0397 |
| 2 | $[PtAuAg_8(dtp)_7(PPh_3)_7 + Ag^+]^+$ | 4685.7891 | 4689.8485 |
| 3 | $[PtAu_2Ag_9(dtp)_7(PPh_3)_6 + Ag^+]^+$ | 4731.7949 | 4733.6183 |
| 4 | $[PtAu_3Ag_{10}(dtp)_7(PPh_3)_5 + Ag^+]^+$ | 4774.9028 | 4776.3952 |
| 5 | $[PtAu_4Ag_{11}(dtp)_7(PPh_3)_4 + Ag^+]^+$ | 4818.8408 | 4818.1578 |
| 6 | $[PtAu_5Ag_{12}(dtp)_7(PPh_3)_3 + Ag^+]^+$ | 4861.8140 | 4861.9558 |
| 7 | $[PtAu_4Ag_9(dtp)_7(PPh_3)_5 + AgPPh_3^+]^+$ | 5123.1948 | 5127.5515 |
| 8 | $[PtAu_5Ag_{10}(dtp)_7(PPh_3)_4 + AgPPh_3^+]^+$ | 5170.2764 | 5170.3283 |
| 9 | $[PtAu_6Ag_{11}(dtp)_7(PPh_3)_3 + AgPPh_3^+]^+$ | 5215.3408 | 5214.1085 |
| 10 | $[PtAu_7Ag_{12}(dtp)_7(PPh_3)_2 + AgPPh_3^+]^+$ | 5255.3872 | 5255.8890 |

**Figure S2.** Positive-ion ESI-MS of **2**.

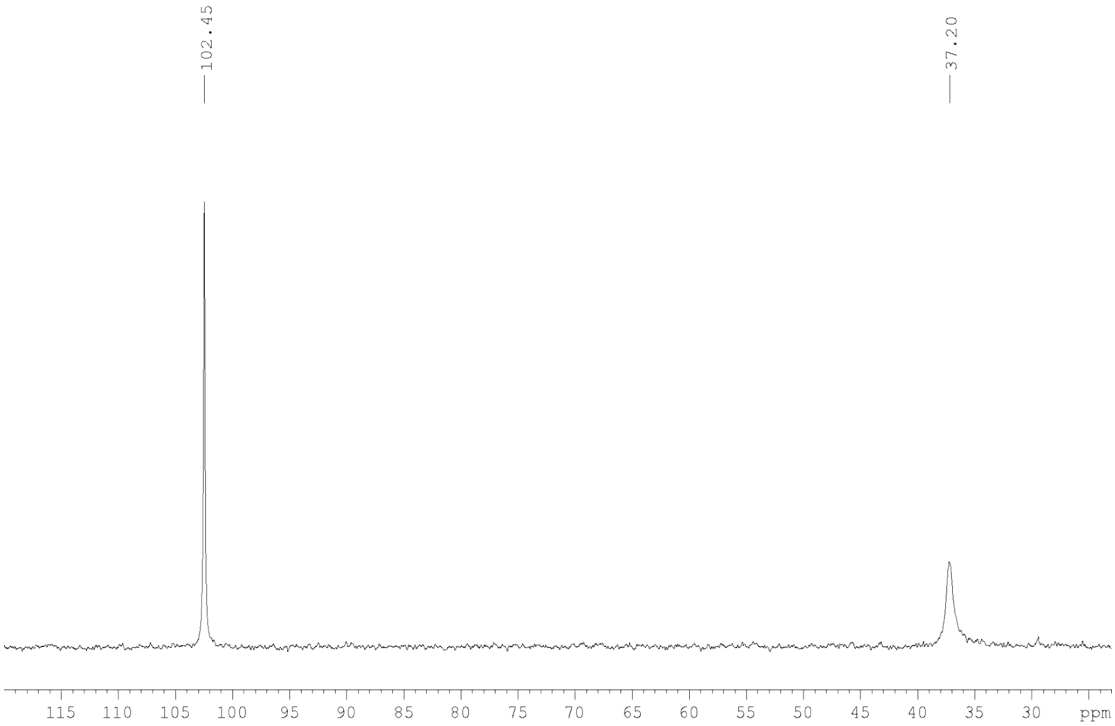


**Figure S3.** $^{31}P\{^{1}H\}$ NMR spectrum ($CDCl_3$) of **1**.

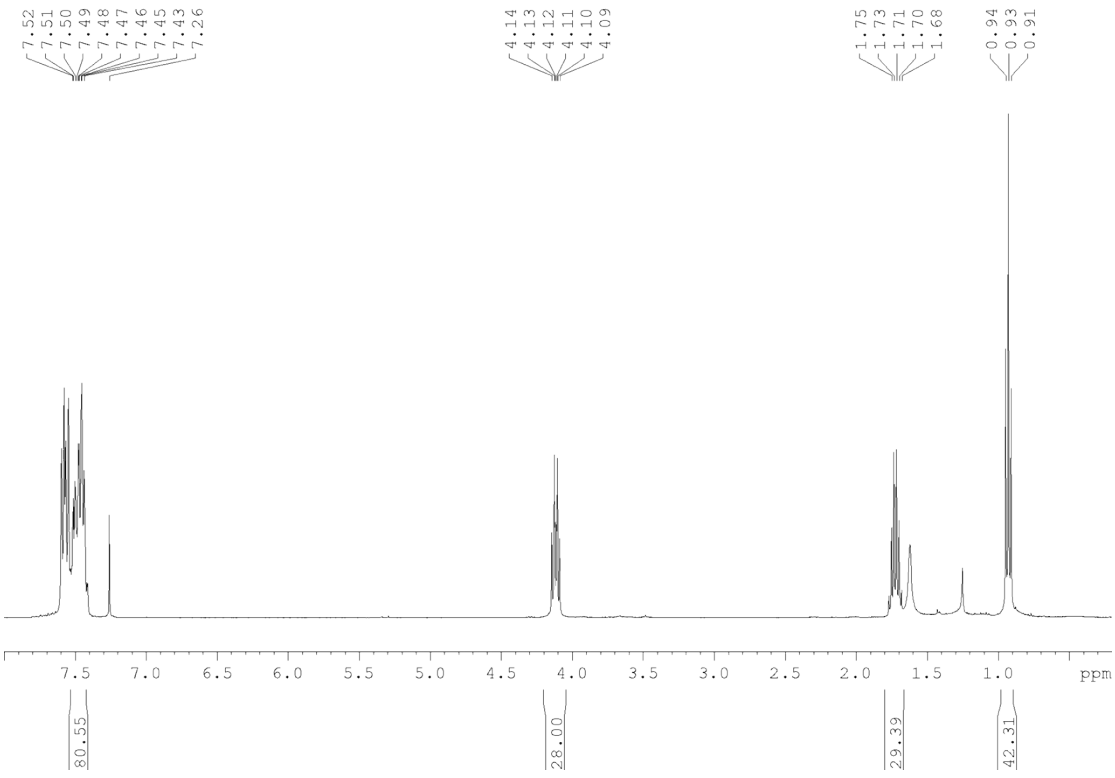


**Figure S4.** $^{1}H$ NMR spectrum ($CDCl_3$) of **1**.

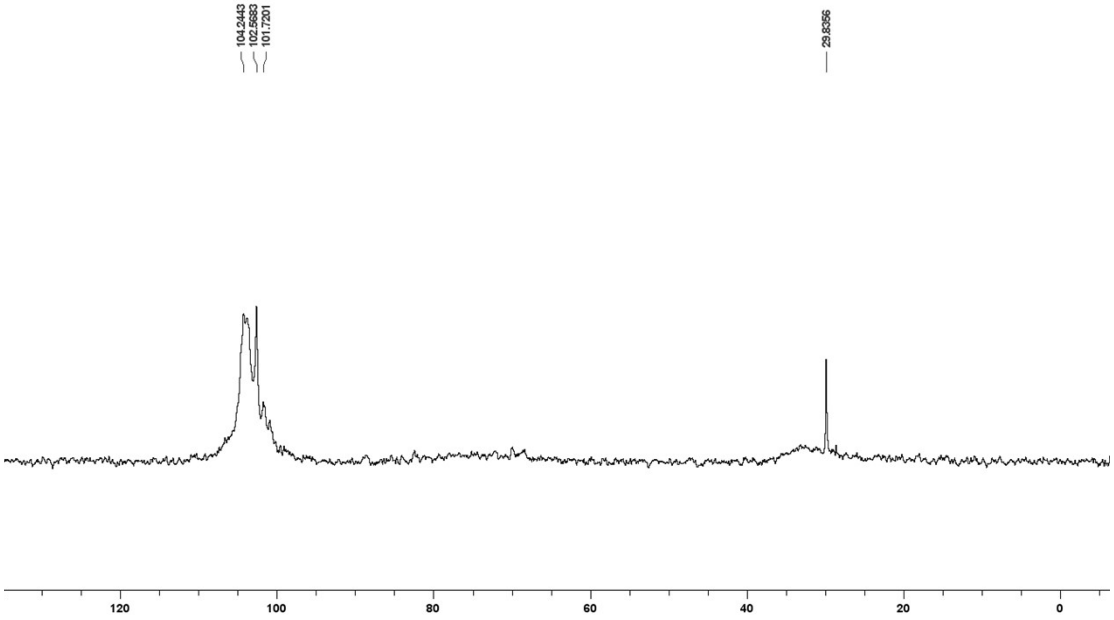


**Figure S5.** $^{31}P\{^{1}H\}$ NMR spectrum ($CDCl_3$) of **2**.

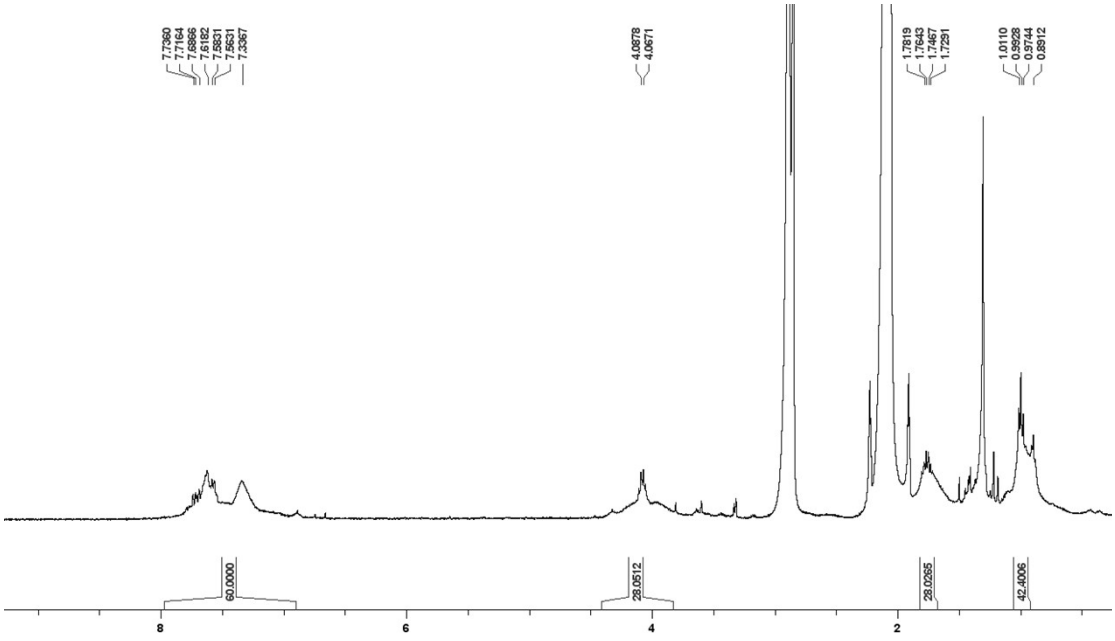


**Figure S6.** $^{1}H$ NMR spectrum ($CDCl_3$) of **2**.

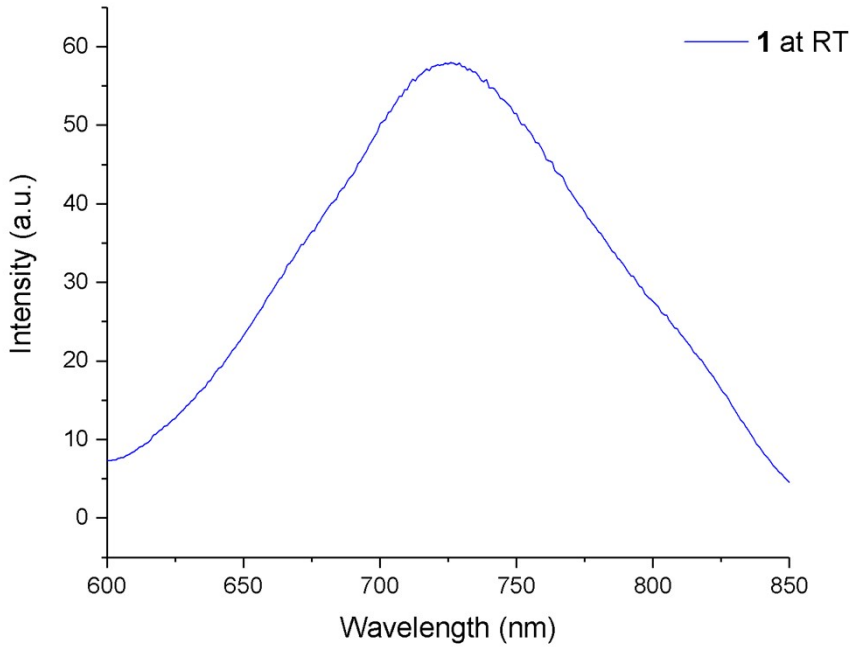


**Figure S7.** The emission spectrum of **1** in 2-MeTHF at room temperature.

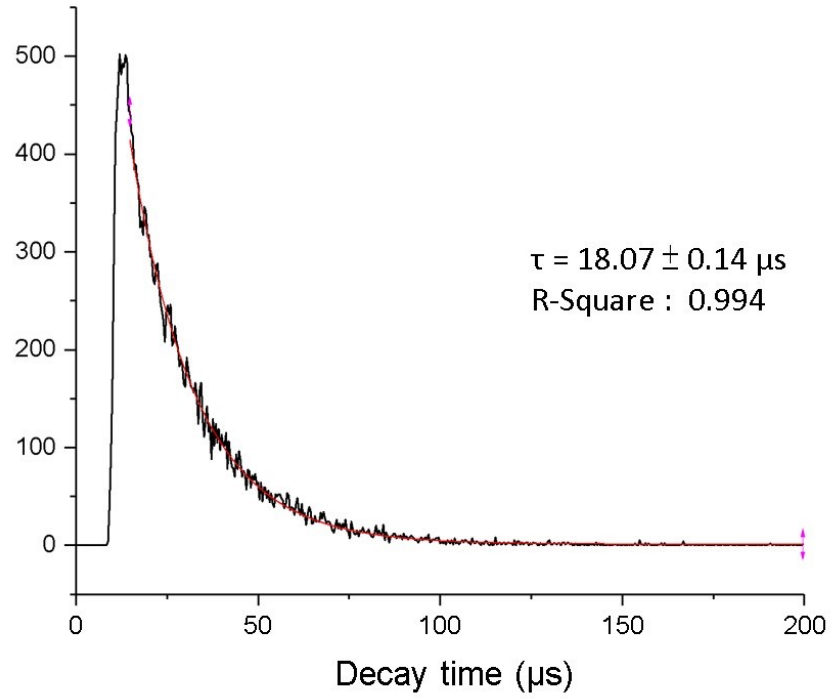


**Figure S8.** Time-resolved photoluminescence spectrum of **1** (2-MeTHF, 77K).

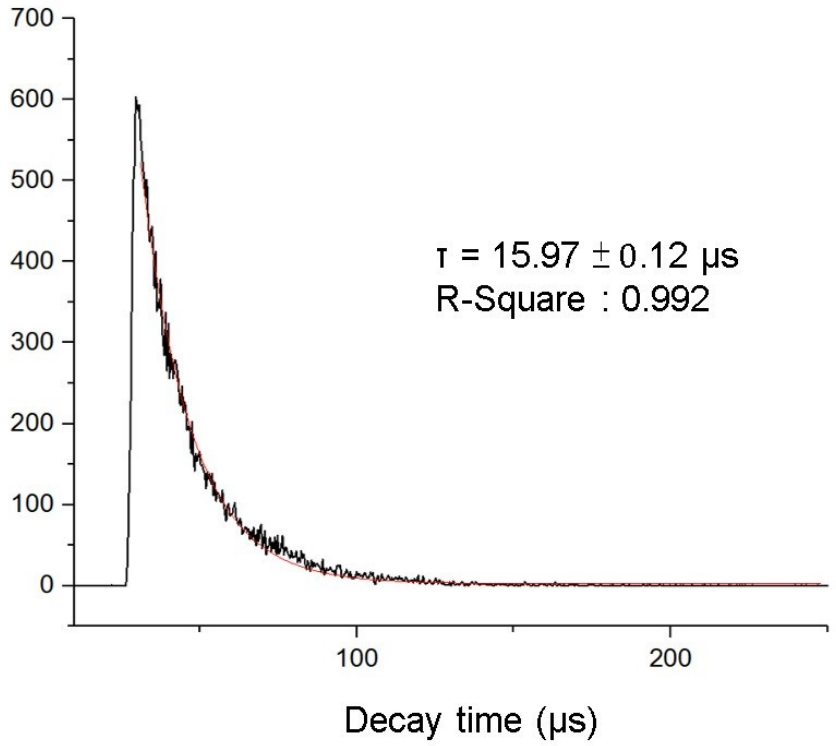


**Figure S9.** Time-resolved photoluminescence spectrum of **2** (2-MeTHF, 77K).

**Table S1.** Selected X-ray crystallographic data of **1** and **2**.

| | $[Au_5Ag_{12}\{S_2P(O^nPr)_2\}_7(PPh_3)_4](PF_6)_2$ | $[PtAu_{4.25}Ag_{10.75}\{S_2P(O^nPr)_2\}_7(PPh_3)_4]$ |
|---|---|---|
| CCDC no. | 2237651 | 2237652 |
| Empirical formula | $C_{114}H_{158}Ag_{12}Au_5F_{12}O_{14}P_{13}S_{14}$ | $C_{114}H_{158}Ag_{10.75}Au_{4.25}O_{14}P_{11}S_{14}$ |
| Formula weight | 5111.12 | 4733.70 |
| Wavelength, Å | 0.71073 | 0.71073 |
| Crystal System | Monoclinic | Triclinic |
| space group | $P2_1/c$ | $P\bar{1}$ |
| a, Å | 30.034(3) | 15.878(3) |
| b, Å | 27.879(3) | 17.651(3) |
| c, Å | 18.1905(18) | 27.489(5) |
| α, deg. | 90 | 89.453(4) |
| β, deg | 97.624(2) | 84.379(5) |
| γ, deg | 90 | 70.430(6) |
| Volume, $Å^3$ | 15097(3) | 7222(2) |
| Z | 4 | 2 |
| Temperature, K | 100(2) | 100(2) |
| $\rho_{calcd}$, $g/cm^3$ | 2.249 | 2.177 |
| μ, $mm^{-1}$ | 6.753 | 7.059 |
| $\theta_{max}$, deg. / Completeness, % | 25.00 / 99.5 | 26.395 / 99.7 |
| Reflections collected / unique | 95474 / 26457 [R(int) = 0.1240] | 29435 / 696 [R(int) = 0.0358] |
| Restraints / parameters | 1519 / 1399 | 696 / 1556 |
| R1[a], wR2[b] [$I > 2\sigma(I)$] | R1 = 0.1084, wR2 = 0.2490 | R1 = 0.0387, wR2 = 0.0863 |
| R1[a], wR2[b] (all data) | R1 = 0.2054, wR2 = 0.3172 | R1 = 0.0529, wR2 = 0.0929 |
| Goodness of fit | 1.104 | 1.024 |
| Largest diff. peak and hole, e/Å $^3$ | 2.809 and -5.870 | 2.805 and -3.028 |

[a] $R1 = \Sigma \mid \Box F_o \Box - \Box Fc \Box \mid / \Sigma \Box F_o \Box$. [b] $wR2 = \{\Sigma[w(F_o^2 - F_c^2)^2]/\Sigma[w(F_o^2)^2]\}^{1/2}$.